PSFC/JA-00-18

Application of Visible CCD Cameras on the Alcator C-Mod Tokamak

C.J. Boswell, J.L. Terry, B. Lipschultz, J. Stillerman

July 2000

Plasma Science and Fusion Center
Massachusetts Institute of Technology
Cambridge, MA 02139 USA

This work was supported by the U.S. Department of Energy, Cooperative Grant No. DE-FC02-99ER54512. Reproduction, translation, publication, use and disposal, in whole or in part, by or for the United States government is permitted.

Submitted for publication to *Review of Scientific Instruments*..

Applications of visible CCD cameras on the Alcator C-Mod tokamak

C. J. Boswell,[†] J. L. Terry, B. Lipschultz, and J. Stillerman
M. I. T. Plasma Science and Fusion Center

(Dated: July 5, 2000)

Abstract

Five 7 mm diameter remote-head visible charge-coupled device (CCD) cameras are being used on Alcator C-Mod for several different diagnostic purposes. All of the cameras' detectors and optics are placed inside a magnetic field of up to 4 T. Images of the cameras are recorded simultaneously using two three-channel color framegrabber cards. Two CCD cameras are used typically to generate two-dimensional emissivity profiles of deuterium line radiation from the divertor. Interference filters are used to select the spectral line to be measured. The local emissivity is obtained by inverting the measured brightnesses assuming toroidal symmetry of the emission. Another use of the cameras is the identification and localization of impurity sources generated by the ion cyclotron radio frequency (ICRF) antennas, which supply the auxiliary heating on Alcator C-Mod. The impurities generated by the antennas are identified by correlating in time the injections seen at the cameras with measurements made with core diagnostics. Fibers whose views aligned with the camera views and whose outputs are coupled to a visible spectrometer are also used to identify the species of the impurities injected.

[†]Electronic address: `boswell@psfc.mit.edu`; URL: `http://www.psfc.mit.edu/people/boswell/`

I. INTRODUCTION

Alcator C-Mod is a high magnetic field, high density, compact tokamak, with a parallel heat flux to the divertor as high as 600 MWm^{-2}.[1] The use of charge-coupled device (CCD) cameras has several advantages over previous methods of measuring visible light emissions on Alcator C-Mod. The benefits include, extremely high spatial resolution, a very large number of viewing chords, use of standard technology (the CCD cameras[2] were purchased off-the-shelf), ease of calibration (a single calibration can be done for all viewing chords), and a large field-of-view, if desired. With a tangential view of the tokamak and the assumption of toroidal symmetry, the cameras have enough viewing chords and spatial coverage for tomographic inversions to be constructed. These inversions are poloidal cross-sections of emission in the tokamak. These cameras are also used to observe both continuous and transient phenomena related to plasma-surface interactions. Since impurity injections degrade the performance of the plasma there is a strong desire to determine the cause of these injections. The cameras on Alcator C-Mod are used to locate the source of these injections, particularly from the ion cyclotron radio frequency (ICRF) antennas.

II. DESCRIPTION

On Alcator C-Mod there are five CCD cameras used in the analysis of either emission distribution or impurity injection. Of these five cameras two view the divertor region and are used to obtain two-dimensional emission profiles, two view ICRF antennas and are used to determine impurity injection location, and a fifth camera views a wide-angle view of the tokamak. All five of the CCD camera are off-the-shelf remote-head "pencil" cameras. The cameras are 7 mm in diameter, 40 mm in length. A 3 m cable connects the camera to the electronics controlling its output. All five cameras are mounted in aluminum holders and affixed to a G-10 platform inside a reentrant tube and behind a shuttered quartz window 10 cm from the last closed flux surface of the Alcator C-Mod plasma. Being mounted in the reentrant tube places the cameras inside the toroidal field coils and magnetic fields of up to 4 T. Fig. 1 shows the location of the cameras in the reentrant tube. Fig. 2 shows the top

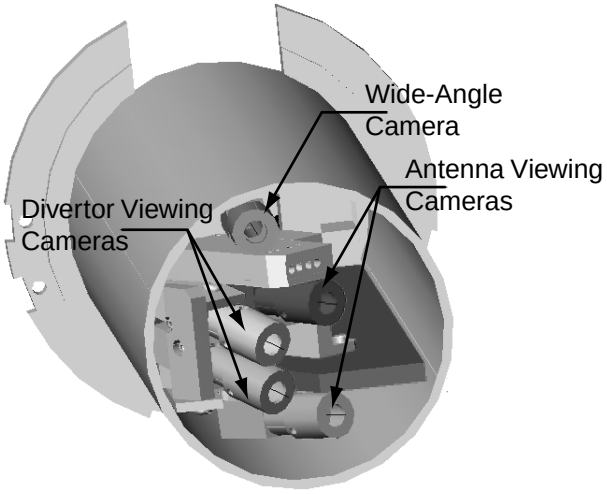

FIG. 1: Five CCD cameras used on Alcator C-Mod, their location and support structure inside the reentrant tube.

view of the tokamak with the typical view each of the cameras.

The positions and views of the cameras are confirmed by fitting identifiable features (e.g., divertor tiles) with known positions inside the machine to their predicted positions in the view. This yields an accuracy of better than 1 millimeter at the tangency point of the chordal views.

The cameras can be spectrally filtered for emission within a particular wavelength range. This is done by placing an interference filter or color-glass filter in front of the lens of each camera. The spectral bandpass of an interference filter is a function of the angle of incidence. This relation is given by

$$\lambda_\theta = \lambda_o \left(1 - \frac{n^2}{2n_*^2} \sin^2 \theta\right), \tag{1}$$

where θ is the angle of incidence, λ_θ is the shifted center of the bandpass, λ_o is the center of the bandpass when $\theta = 0$, n is the index of refraction in the medium surrounding the interference filter, and n_* is the effective index of refraction in the interference filter.[3] Using Eq. (1) interference filters must be chosen such that the spectral line of interest be within the bandpass for all possible viewing angles of the cameras.

In the case where the desired measurement is an emission line, two calibrations are done,

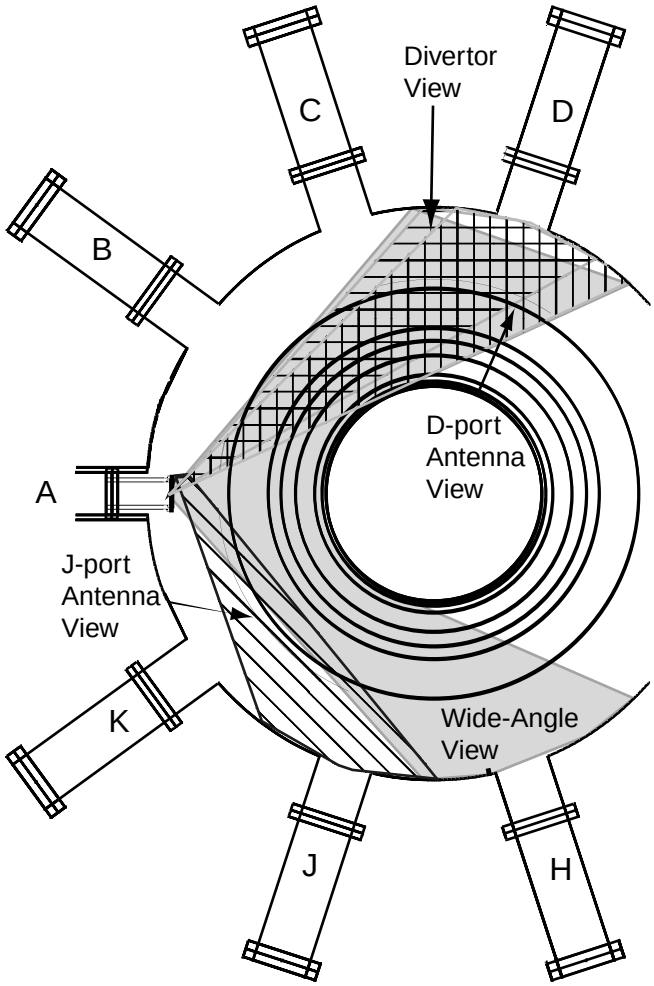

FIG. 2: The view of each of the five cameras, labelled accordingly.

1) to determine the transmission function over the entire field-of-view of the camera and 2) to determine the absolute sensitivity of each camera chord measured by each pixel to a given incident energy for a given filter/lens combination. The first calibration is easily done for H_α, H_β, or H_γ (D_α, D_β, or D_γ), by sweeping a hydrogen (deuterium) lamp across the view of camera and mapping the measured brightness as a function of pixel location on the CCD chip. The next calibration is the absolute calibration and is done by mapping the measured brightness recorded by the camera when observing a calibrated uniform brightness source to the pixel value obtained for the given brightness. This is done knowing the transmission function of the desired filter.

All five cameras are recorded simultaneously on two personal computers. Each computer is equipped with a color frame-grabber that is set-up to record three cameras (instead of

three colors). The output from the CCD cameras is in NTSC format, which limits the frame rate to 30 per second. In this format a frame is made of two interlaced fields recorded at twice the frame rate of the camera. Therefore each recorded frame has two recorded time steps (one in each field) and the fastest information can be obtained is 60 Hz.

III. DATA ANALYSIS

The two cameras viewing the divertor are used to obtain two dimensional emission profiles of the divertor. The two dimensional profiles of the emissivities are generated using an infinitely thin chord approximation and assuming toroidal symmetry. It is assumed that each camera pixel's view is a thin chord projected through the focus of the camera lens system. The approximation is justified as long as the actual projection of the camera pixel remains much smaller than the dimensions of the emission grid boxes. Using an 8mm focal length lens, the projections of the camera pixels are less than 1 mm wide at the plane of tangency and the inversion box size used is 0.5 cm wide.

The emissivity, ϵ, is derived from the brightness, b, measured by the camera pixels (with the thin chord approximation). The brightness is

$$b = \frac{1}{4\pi} \int \epsilon \, ds, \tag{2}$$

where s is the distance along camera pixel view. To solve for the emission profile, Eq. (2) is discretized into the following form,

$$b_i = \frac{1}{4\pi} \epsilon_j \Delta s_{ij}, \tag{3}$$

where the index i represents the quantity for the i^{th} camera pixel, and Δs_{ij} is the chordal length through ϵ_j for chord i, and the repeated subscript implies a sum. Of the possible 307 200 pixels chords only $\sim$ 3000 are used to obtain the emissivity profiles of $\sim$ 2500 grid elements. In these cases less than 200 chords pass through any given emission grid element. This gives sufficient coverage of each emission grid element while allowing the matrix Δs_{ij} to be sparse enough that Eq. (3) can be solved, in a least squares sense, using the conjugate-gradient method [4].

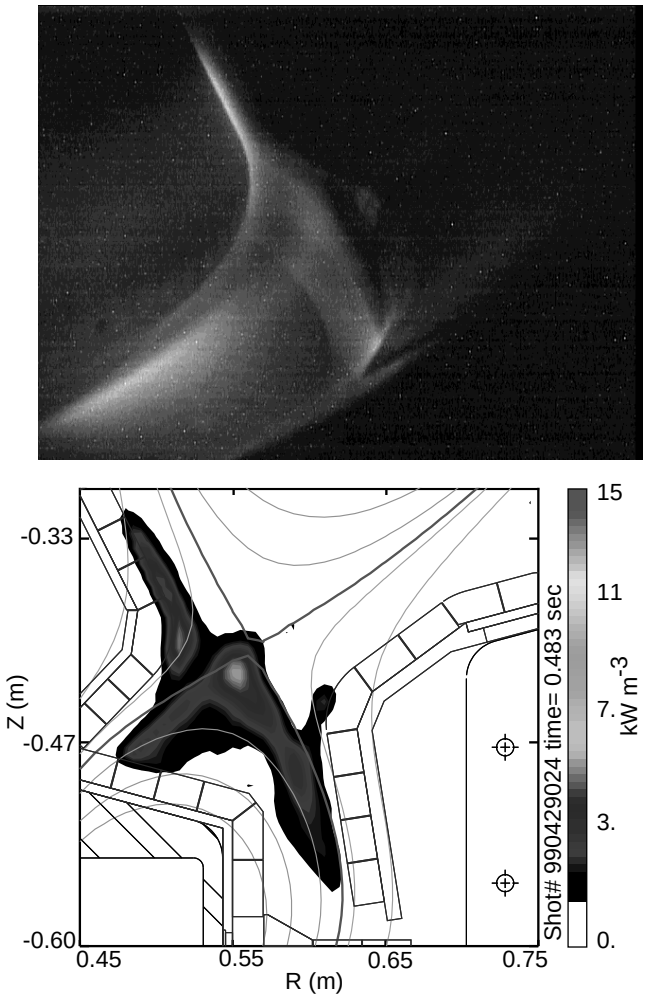

FIG. 3: Recorded brightness image of D_γ emission from a CCD camera and its corresponding emissivity profile.

Using this mathematical construct and algorithm for solving the problem, the emissivities are readily generated. Fig. 3 shows the recorded brightness image and its corresponding emission profile using this technique. As a check on the accuracy of the inverted profiles and on the justification of the assumption of toroidal symmetry, the recorded brightnesses from the visible spectrometer[5] and the photo-diode arrays[6] on Alcator C-Mod are compared to brightnesses generated by integrating the same chordal view through the inverted emissivity profile. The two agree to within 10 percent.

A source of error can arise from reflections seen by the camera or other spectroscopic diagnostics. These reflections when unaccounted for in Eq. (3) can result in incorrect emission

profiles. Unlike other devices with graphite or carbon-composite internal armor, Alcator C-Mod's inner wall and divertor armor is boronized molybdenum. As such, reflections can occur. A comparison of CCD brightness along nearly identical chords, one viewing the flat surface of a divertor tile and the other viewing the spacing between tiles (a non-reflecting surface) yields a $\leq 10\%$ difference. In addition, care is taken when generating the inversions to minimize the effect of the reflections by choosing camera pixels that view mostly the spaces between the tiles. It is also the case that the diode arrays and visible spectrometer view different reflections than the CCD cameras. Even so, the agreement between the absolute brightnesses measured by the different diagnostics is quite good. Therefore, it is believed that the reflections do not influence the results significantly.

The recorded images from the cameras viewing the ICRF antennas are used to locate spatially the observed injections from the antennas. Locating the injections is done by determining where the injections are with reference to the identifiable features (protection tiles, antenna structure, etc.) and correlate it in time with other spectroscopic diagnostics.

IV. RESULTS

The divertor cameras in the configuration described above have been used to observe the distribution of deuterium emission during detachment and measure volume recombination in the divertor. The antenna viewing cameras have been used to locate impurity injections from the ICRF antennas.

A Distribution of deuterium emission during detachment

The plasmas used to investigate deuterium emission in the divertor had a plasma current of 1 MA, toroidal magnetic field of 5.4 T, and a diverted single null with the ion ∇B drift in the direction of the divertor. The line-averaged densities in these discharges were ramped up from $1 \times 10^{20}\mathrm{m}^{-3}$ to $3.6 \times 10^{20}\mathrm{m}^{-3}$. The divetor viewing cameras in this instance were filtered for $\mathrm{D}_\alpha(n = 3 \rightarrow 2)$ and $\mathrm{D}_\gamma(n = 5 \rightarrow 2)$ radiation.

It has previously been shown that the D_γ emission is related to the number of complete (i.e., to the ground state) recombinations in the low temperature ($\lesssim 1$ eV) and high density ($\gtrsim 1 \times 10^{21}$ m^{-3}) plasma conditions that typically occur in detached plasmas.[7] This gives a direct method for observing regions of volume recombination before, during and after a detached divertor is formed. Fig. 4 shows two profiles of D_γ emission, 1) as the divertor plasma begins to detach from the outer divertor plate and 2) at a time when the divertor is deeply detached (i.e., when the current to the divertor plates has decreased by an order of magnitude.). At the onset of detachment, a region of strong D_γ emission exists at the strikepoint of the outer divertor leg. As the detachment deepens the D_γ emission, and hence the recombining region, expands up the outer leg until it reaches the x-point. If the detachment of the outer leg is pushed further, (e.g., by continuing to increase the plasma density) the recombining region extends into the confined plasma above the x-point, and eventually results in a disruption.[8, 9]

B Evaluation of the magnitude of recombinations

Using the two-dimensional profiles of D_γ emission and the temperature and density measurements measured using deuterium Balmer spectra from multiple chords viewing the divertor region, it is possible to determine the magnitude of the volume recombination in the divertor. The temperatures in the recombining regions are determined by fitting the high-n Balmer spectra to a Saha distribution, and the electron densities are determined by measuring the Stark broadening of the $n = 6, 7, 8 \rightarrow 2$ deuterium lines.[10] Fig. 4 shows the spectrometer chords from which spectra are recorded.

The spectral data are line integrations through different divertor regions. The temperature and density measurements can be spatially localized by recognizing that most of the line integrated photons come from the region where the emission is greatest. The distribution of the emission determines how well localized the measurement can be. The chordal measured n_e and T_e have been attributed to the peak in the emission along the viewing chord. Using these two-dimensional profiles, the emission from which the temperature and density mea-

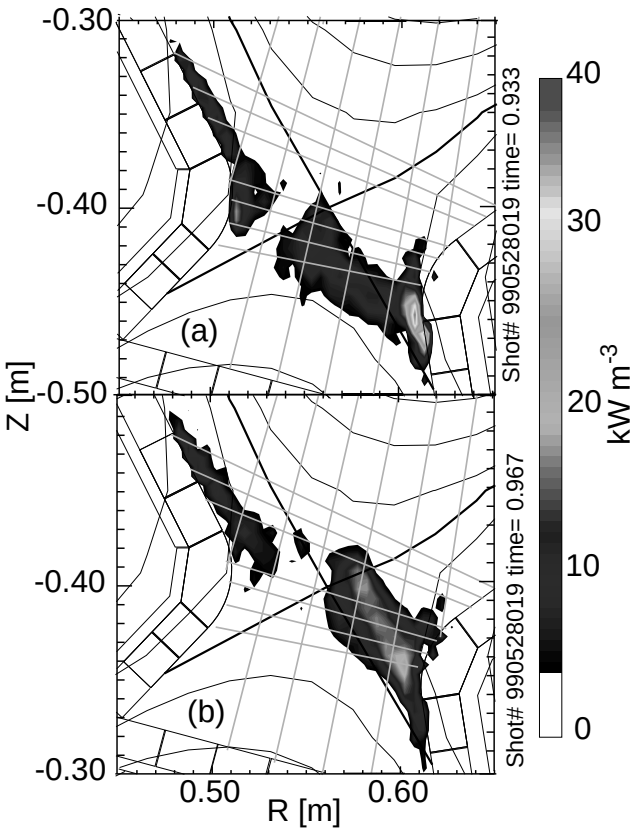

FIG. 4: Two D_γ emission profiles, (a) in the beginning of partially detached conditions and (b) during deeply detached operation. The straight lines show views used by the visible spectrometer.

surements are made, can be spatially localized, creating a rough profile of temperature and density in the divertor. Terry, *et al.*[7] discusses and defines the number of recombinations per D_γ photon concept that is used here to determine the rate of volume recombination. The recombinations per D_γ photon curves show a strong temperature dependence to T_e, but a less than linear dependence upon n_e.

Using the D_γ emission profile from Fig. 4(b), the temperature and density measurements from the side viewing chords of the visible spectrometer from Fig. 4, and the recombinations per D_γ photon curves the recombinations per unit volume per unit time have been measured. Fig. 5 shows the location and the relative magnitudes of the volumetric recombinations per unit time. The maximum value measured is $5.18\times10^{24}\mathrm{m}^{-3}\mathrm{s}^{-1}$ and the lowest value measured was $2.10 \times 10^{24}\mathrm{m}^{-3}\mathrm{s}^{-1}$. These values can equal or be greater than the particle current to

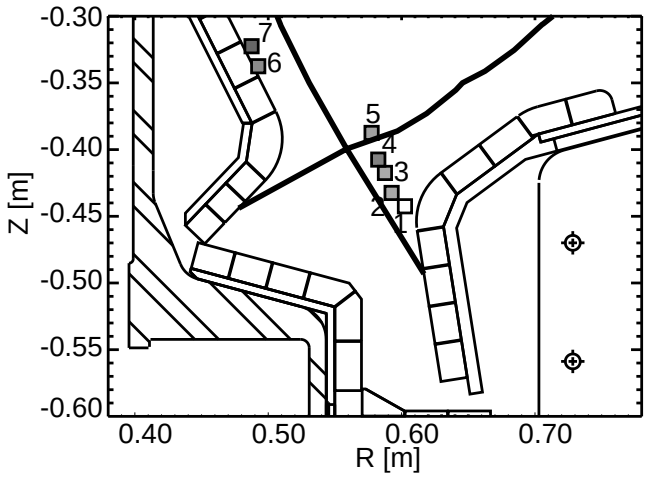

FIG. 5: Location and relative magnitudes of the volumetric recombinations per unit time. The maximum value measured is $5.18 \times 10^{24}\mathrm{m}^{-3}\mathrm{s}^{-1}$ and the lowest value measured was $2.10 \times 10^{24}\mathrm{m}^{-3}\mathrm{s}^{-1}$

the divertor through these regions.

C Location and identification of impurity injections from the ICRF antennas

Fig. 6 shows the recorded frame of an upper corner of an ICRF antenna. The nearly horizontal bars on the right side of the image are the Faraday shield, behind which are the antenna straps (not visible). The vertical tiles on the lower center of the image are the side molybdenum protection tiles. The top molybdenum protection tiles are located beneath the bright white region on the right side of the image. With no filter the cameras' spectral response is from 380nm to 1100nm. In this unfiltered configuration, the cameras occasionally observe intense localized emission coming from the space between the molybdenum protection tiles around the antennas. We hypothesize that the emission accompanies the ablation of material from these tiles.

Colinear to the cameras viewing the ICRF antennas are visible spectrometer views. The visible spectrometer is used to determine the species of the injections from the ICRF antennas by the identification of specific spectral lines. These injections occurred primarily at the top and the bottom protection tiles and rarely on the side protection tiles. Fig. 6 shows a

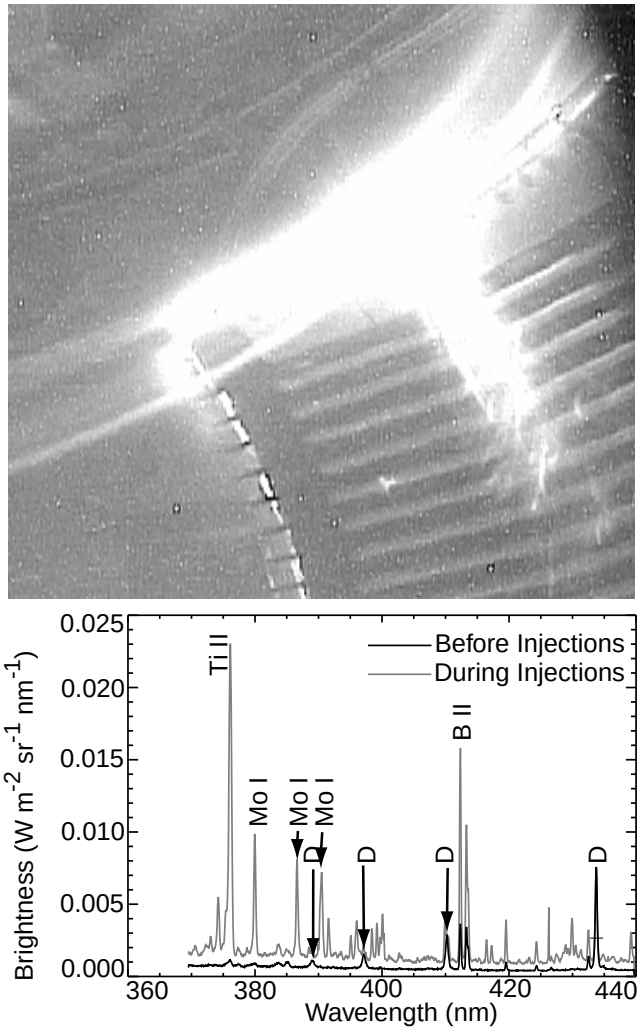

FIG. 6: A typical recorded frame of an injection from the ICRF antennas along with the corresponding spectrum compare to a spectrum from before the injection.

recorded frame of an injection along with the corresponding spectrum associated with the injection compared to a spectrum from before the injection. The dominant species identified during the event is molybdenum with titanium occurring in some cases. The identification of these impurities coming from the protection tiles is consistent with the material make-up of the protection tiles. The boron impurity is also expected since the entire first wall of the machine is coated routinely with a several micron-thick layer of boron.

V. SUMMARY

Alcator C-Mod has five CCD cameras with various views of the tokamak discharge. Two of the cameras are used for viewing the divertor emission and generating two-dimensional emission profiles, two are used to locate and identify impurity injections from the ICRF antennas, and one is used to provide a wide-angle view of the tokamak.

Two-dimensional profiles of deuterium emission have been generated using the two CCD cameras with nearly identical, tangential views of the divertor. These cameras are filtered for deuterium emission using interference filters. The cameras are recorded simultaneously using a video-capture board installed on a personal computer. The CCD cameras are absolutely calibrated. The profiles are generated by inverting the images, using the assumptions of toroidal symmetry and the thin chord approximation. Since the geometry matrix used is sparse, the conjugate-gradient method is used to solve for the emissivity profile. The two-dimensional profiles generated from the camera images were compared with chordal brightness measurements from other diagnostics and found to agree essentially. This agreement implies that the profiles are correct.

Emission profiles have been generated for the partially detached and deeply detached divertor operation. The partially detached case shows a strong localized region of D_γ at the strikepoint, while the deeply detached case shows the D_γ region extending up the outer leg to the x-point. With the profiles of D_γ emission, temperature and density measurements from a visible spectrometer, and the recombinations per D_γ photon curves, a measure the volumetric recombination can be determined during detached divertor operation. The two-dimensional profiles also spatially localize, to the peak emission region, the temperature and density measurements obtained spectroscopically by chordal views.

Two cameras are used to locate the impurity impurity generation from the ICRF antennas on Alcator C-Mod. The impurities were observed to originate primarily from spaces between the protection tiles on both the top and the bottom of the ICRF antennas. Using visible spectra measured along fiber views of the antenna, it was found that the dominant impurities from these injections are molybdenum and titanium.

VI. ACKNOWLEDGEMENTS

This work was supported by the U. S. Dept. of Energy under grant #DE-FC02-99ER54512.

REFERENCES

[1] I. H. Hutchinson, R. Boivin, F. Bombarda, P. Bonoli, S. Fairfax, C. Fiore, J. Goetz, S. Golovato, R. Granetz, M. Greenwald, S. Horne, A. Hubbard, *et al.*, Phys. Plasmas **1**(5), 1511 (1994).

[2] Toshiba IK-SM43H 7mm Camera Head with Toshiba IK-CU43A Camera Control Unit.

[3] H. A. Macleod, *Thin-Film Optical Filters* (American Elsevier Publishing Company, Inc., New York, 1969).

[4] C. C. Paige and M. A. Saunders, ACM-TOMS **8**(1), 43 (1982).

[5] D. Lumma, J. L. Terry, and B. Lipschultz, Phys. Plasmas **4**(7), 2555 (1997).

[6] J. L. Terry, J. A. Snipes, and C. Kurz, Rev. Sci. Instrum. **66**(1), 555 (1995).

[7] J. L. Terry, B. Lipschultz, A. Y. Pigarov, S. I. Krasheninnikov, B. LaBombard, D. Lumma, H. Ohkawa, D. Pappas, and M. Umansky, Phys. Plasmas **5**(5), 1759 (1998).

[8] B. Lipschultz, J. L. Terry, C. J. Boswell, S. I. Krasheninnikov, B. LaBombard, and D. Pappas, J. Nucl. Mater. **266–269**, 370 (1999).

[9] B. Lipschultz, J. L. Terry, C. J. Boswell, J. A. Goetz, A. E. Hubbard, S. I. Krasheninnikov, B. LaBombard, D. Pappas, C. S. Pitcher, F. Wising, and S. Wukitch, Phys. Plasmas **6**(5), 1907 (1999).

[10] B. Lipschultz, J. L. Terry, C. Boswell, A. Hubbard, B. LaBombard, and D. A. Pappas, Phys. Rev. Lett. **81**(5), 1007 (1998).